ACTA UNIVERSITARIA
Multidisciplinary Scientific Journal

| VOLUMEN 29 | 2019 |
ISSN online 2007-9621
http://doi.org/10.15174/au.2019.2036

Application of spheroidal agglomerates of γ-Al_2O_3 in the fluoride removal from aqueous medium

Aplicación de aglomerados esferoidales de γ-Al_2O_3 en la remoción de fluoruro de medio acuoso

Rafael Romero Toledo[1]*, Víctor Ruiz Santoyo[2], Ulises Zurita Luna[3], Gustavo Rangel Porras[1], Merced Martínez Rosales[1]

[1]Universidad de Guanajuato, División de Ciencias Naturales y Exactas, Noria Alta S/n, Col. Noria Alta, Guanajuato, Gto., C.P. 36050, México.
E-mail: r.romerotoledo@ugto.mx
[2]Facultad de Ingeniería Química, Benemérita Universidad Autónoma de Puebla.
[3]Facultad de Ingeniería Química, Universidad Michoacana de San Nicolás de Hidalgo.
*Corresponding author.

Abstract

A spheroidal agglomerate γ-Al_2O_3 adsorbent obtained from pseudoboehmite for effective removal of fluoride from aqueous medium was investigated in the present study. The surface properties were characterized by several techniques: XRD, physisorption of N_2, FE-SEM/EDS, ^{27}Al NMR, FT-IR Pyridine adsorption, PZ and particle size. Batch experiments were conducted and they were compared with a commercial activated alumina (AA). The process was carried out at pH 5, 7, and 9, then at 25 and 35 ºC. Batch experimental results indicated that the spheroidal agglomerates of γ-Al_2O_3 remove up to 15 mg/g with a higher adsorption capacity than AA of 13 mg/g, at pH 5, studied at 25 and 35 °C. The F^- adsorption processes in γ-Al_2O_3 and AA followed the pseudo-first-order kinetics and the Langmuir isotherm. The results showed an adsorbent effective for removal of F−.

Keywords: Fluoride; γ-Al_2O_3; spheroidal agglomerates; adsorbent; water.

Resumen

En el presente estudio se investigó un adsorbente aglomerado esferoidal de γ-Al_2O_3 obtenido a partir de pseudoboehmita para la eliminación eficaz de fluoruro de un medio acuoso. Las propiedades superficiales se caracterizaron por diversas técnicas: XRD, fisisorción de N_2, FE-SEM/EDS, RMN ^{27}Al, adsorción de piridina por FT-IR, PZ y tamaño de partícula. Se llevaron a cabo experimentos en lotes y se compararon con una alúmina activada comercial (AA). El proceso se llevó a cabo a pH 5, 7 y 9, a 25 y 35 ºC. Los resultados experimentales indicaron que los aglomerados esferoidales de γ-Al_2O_3 eliminan hasta 15 mg/g, con una capacidad de adsorción mayor que AA de 13 mg/g, a pH 5, estudiados a 25 y 35 ºC. El proceso de adsorción de F^- en γ-Al_2O_3 y AA siguió la cinética de pseudo-primer orden y la isoterma de Langmuir. Los resultados muestran un adsorbente eficaz para la eliminación de F^-.

Palabras Clave: Fluoruro; γ-Al_2O_3; aglomerados esferoidales; adsorbente; agua.

Recibido: 27 de julio de 2017 **Aceptado:** 26 de septiembre de 2018 **Publicado:** 9 de octubre de 2019

Como citar: Romero-Toledo, R., Ruiz-Santoyo, V., Zurita-Luna, U., Rangel-Porras, G., & Martínez-Rosales, M. (2019). Application of spheroidal agglomerates of γ-Al_2O_3 in the fluoride removal from aqueous medium. *Acta Universitaria 29*, e2036. doi. http://doi.org/10.15174.au.2019.2036

Introduction

Fluoride contamination of groundwater by natural as well as anthropogenic sources is a major problem worldwide (Cheng, Meng, Jing & Hao, 2014). The maximum contaminant level (MCL) with fluoride in drinking water, established by the US EPA, is 4 mg/L (Tang, Guan, Su, Gao & Wang, 2009). The World Health Organization (WHO) guideline value of fluoride in drinking water, which was also adopted by the Mexican legislation, is 1.5 mg/L (*Diario Oficial de la Federación* [DOF], 2001; WHO, 2004). Above 1.5 mg/L, mottling of teeth may occur to an objectionable degree. Concentrations between 3 mg/L and 6 mg/L may cause skeletal fluorosis. The continuous consumption of water with fluoride in exceeding levels of 10 mg/L can result in crippling fluorosis (Yeung, 2008). Fluoride is one of the four most important polluting chemicals, in addition to arsenic, nitrate, and chromium (VI), which cause a large scale of health problems to humans through drinking water exposure (Tang *et al*., 2009).

It is significant to consider that fluorine content in groundwater is above the WHO standards in many countries and regions. Excessive fluoride concentrations have been reported in groundwaters that belong to more than 10 developed and developing countries (Arora & Maheshwari, 2006; Cheng *et al*., 2014), including Mexico, where several states are facing fluorosis problems. The most affected states are Aguascalientes, Coahuila, Chihuahua, Durango, Guanajuato, Hidalgo, Jalisco, San Luis Potosi, Sonora, and Zacatecas. In the Bajio region, the fluoride content is found in the range 2.5 mg/L-5.5 mg/L. In this region, about 75% of the people consume groundwater for drinking purposes, exceeding the WHO guidelines (Rosales, Coreño & Nava, 2018). Worldwide, it is estimated that more than 70 million people are suffering from fluorosis (Sehn, 2008).

Fluoride can be removed from water by employing a number of processes, including adsorption and biosorption (Chatterjee & De, 2014); ion-exchange (Rogoziński, Tyszkiewicz, Karasiński, Żelechower & Szala, 2016); chemical precipitation, which may include electro-coagulation/flotation (Drouiche *et al*., 2012); and membrane processes, such as reverse osmosis (Shen, Richards & Schäfer, 2016), dialysis (Kir & Alkan, 2006), nano-filtration (Jadhav, Marathe & Rathod, 2016), and electrodialysis (Arahman, Mulyati, Lubis, Takagi & Matsuyama, 2016). Most methods for removing fluoride have drawbacks, including high-initial costs, lack of selectivity, low capacity, and difficulty in operation or regeneration.

Activated alumina (AA) has been used as an effective and inexpensive adsorbent for fluoride removal (Leyva-Ramos *et al*., 2008; Rafique, Awan, Wasti, Qazi & Arshad, 2012), that is because of its strong affinity for fluoride, availability in the market (Shen *et al*., 2016), high thermal stability (Xu *et al*., 2017), mechanical strength, porosity, large surface area, and surface chemical properties that can be either acidic or basic, depending on the transition alumina structure and the degree of hydration/hydroxylation of the surface.

Adsorption is one of the most commonly used techniques for fluoride removal from water, and the effectiveness of adsorption techniques is greatly dependent on the physical-chemical properties of the adsorptive materials. A wide variety of adsorption materials has been tested for the removal of fluoride from water, such as montmorillonite (Tor, 2006), bentonite (Ma, Shi, Zheng, Ma & Gao, 2011), hydrocalumite (Guo & Tian, 2013), bauxite and charcoal (Singh, Singh & Singh, 2016), biopolymer (Singh, Singh & Singh, 2016), Al_2O_3/CNT (Li *et al*., 2001), activated alumina (AA) (Ghorai & Pant, 2005), bone char (Nigri, Bhatnagar & Ferreira-Rocha, 2017), zeolite (Gómez, Pérez, García, Chebude & Díaz,2013), as well as rice husk and calcium (Bhatnagar, Kumar & Sillanpää, 2011). There are other materials that have been reported as useful for fluoride removal. However, their low adsorption capacities and poor adsorption kinetics demonstrate they still need improvement. An ideal adsorbent should have uniformly accessible pores, a high surface area, and physical-chemical stability. Due to that, adsorption processes involve the passage of the water through a contact bed where fluoride is removed by ion exchange or surface chemical reaction.

The objective of this work is to compare the removal of fluoride ions from water using a γ-Al_2O_3 synthesized-agglomerate and a commercial AA, as well as the effects of the solution pH and temperature in the adsorption capacity. The average particle diameter of both materials was 3 mm, and they were systematically characterized with XRD, adsorption/desorption of N2, FE-SEM/EDS, ^{27}Al MAS NMR, FT-IR pyridine adsorption, and zeta potential analysis and particle size. That is to understand their physical-chemical properties and the adsorption of fluoride in the alumina.

Materials and Methods

Synthesis and pseudoboehmite agglomeration

In the present study, the starting materials to obtain hydrated alumina (γ-Al_2O_3) are $Al_2(SO_4)_3$•$18H_2O$, with a purity of 95% (by weight, wt.), technical grade, Alfa-Omega Chemical S. A., HNO_3 (karal 70%), C_6H_{14} (J. T. Baker 99.8%), NH_4OH (Karal 30%), and anhydrous NH_3 gas (Praxair, 99.98% [wt.]) as precipitant.

The preparation procedure flow chart is depicted in figure 1. $Al_2(SO_4)_3$•$18H_2O$ was dissolved into deionized water and filtered for the removal of insoluble impurities. The precursors were prepared by dropping the saturated solution of aluminum sulfate into the solution of water and ammonia gas. That was done under rigorous magnetic stirring at a temperature range of 50 °C-70 ºC. The precipitated solution was filtered, and the precipitate of pseudoboehmite was rinsed with distilled water two times and then dried at 110 °C for 12 h. The agglomeration of pseudoboehmite in solid spheres of 3 mm diameter was obtained from a colloidal solution. The colloidal solution was prepared using pseudoboehmite, nitric acid, and distilled water. This solution was then dripped into a glass column with 15 mL of C_6H_{14} and 25 mL of NH_4OH for making the agglomeration. The phase change from pseudoboehmite agglomerates to γ-Al_2O_3 was performed by a thermal treatment at 550 °C for 6 h. The chemical reactions (1), (2), and (3) occurred during the synthesis and the gamma phase was obtained:

Precipitation step:

$$Al_2(SO_4)_3 + 6NH_4OH \rightarrow 2AlOOH + 3(NH_4)_2SO_4 + 2H_2O \quad (1)$$

Calcination step:

$$2AlOOH \rightarrow \gamma - Al_2O_3 + H_2O \quad (2)$$

The AA used in this study is commercial spherical with a diameter of 3 mm (Alquimia Mexicana S. de R. L.).

ISSN online 2007-9621

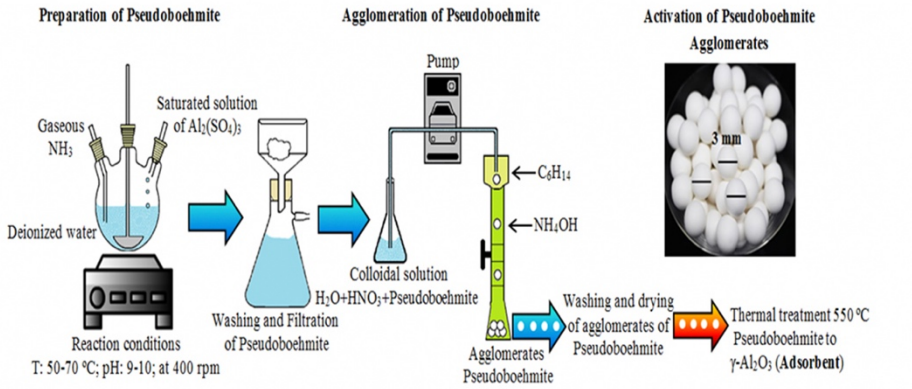

Figure 1. Synthesis and process of agglomeration of Pseudoboehmite (precursor of γ-Al_2O_3).
Source: Author's own elaboration.

Surface characterization of the adsorbents

The γ-Al_2O_3 and AA samples were dispersed into distilled water. The solutions pH were adjusted to the following ranges for analysis: between 2 mM and 12 mM when using KCl, and 10 mM when using NaOH. The zeta potential and particle size were analyzed using an electroacoustic technique with a particle size analyzer (AcoustoSizer II, ESA; Colloidal Dynamics, USA) at 25 °C ± 0.2 °C. The textural properties were characterized by N_2 adsorption (Micromeritics, ASAP 2010). The samples were vacuum degassed at 200 °C for 3 h. Nitrogen adsorption isotherms were measured at a liquid N_2 temperature (77 K) and N_2 pressures ranging from 10^{-6} P/P_0 to 1.0 P/P_0. The surface area was calculated according to the Brunauer–Emmett–Teller (BET) method, and the pore size distribution was obtained according to the Barret–Joyner–Halenda (BJH) method. The crystalline properties of the samples were determined at room temperature by using X-ray powder diffraction. A Siemens D-500 diffractometer equipped with a CuKα radiation anode was used for these measurements, under the following conditions: a sweep of 5°-80º at an angle of 2θ, with a wavelength of k = 1.54 Å, a current of 30 kV, and a current of 20 mA. Solid-state nuclear magnetic resonance (NMR) measurements were made with a Bruker Avance III HD 400 spectrometer in a nominal field of 9.4 T at a Larmor frequency of 104 MHz. The ^{27}Al spectra were observed using a magic angle spinning (MAS) probe. For this process, rotors of 4 mm were used, as well as a rotation frequency of approximately 11 kHz, using as reference a solid sample of $Al(NO_3)_3$• $9H_2O$ (^{27}Al, d = 0.0 ppm). The nature of acid sites was determined by pyridine adsorbed Fourier transformed infrared (pyridine FT-IR) spectroscopy in a FT-IR Nicolet 470 instrument with a resolution of 1 cm^{-1}. The samples were dehydrated at 300 °C for 1 h under vacuum. This was followed by adsorption of purified pyridine at room temperature. Then, the sample was evacuated at room temperature and later at 200 °C. The pyridine-adsorbed IR spectra were recorded. The surface morphology was examined using JEOL JSM-7600-F Field-Emission scanning electron microscopy. This was equipped with an energy dispersive X-ray spectrometer (FE-SEM/EDS) to determine the chemical composition.

Batch adsorption experiments

F^- adsorption kinetics experiments were conducted by mixing suspensions containing 10 mg/L, 30 mg/L, 50 mg/L, 100 mg/L, and 150 mg/L of fluoride ion in deionized water with 0.3 grams of adsorbent material to the levels of pH of 5, 7, and 9, which was adjusted with hydrochloric acid. Samples were left for five days at different temperatures (25 °C and 35 °C); this was because the groundwater temperature varies from 25 °C to 50 ºC. The highest temperatures are located near faults and fractures. High temperatures match with

ISSN online 2007-9621

the highest groundwater concentrations of As and F^- in Guanajuato, Mexico (Morales, Villanueva-Estrada, Rodríguez & Armienta, 2015). The samples in solution were analyzed immediately at the desired mixing time. The residual F– concentration in solution samples was measured using a fluoride selective electrode (Thermo Scientific Orion 4-Star Plus). That was in accordance with the standard method (Wang *et al.* 2014). After five days, the solution was filtered, and the final concentrations of fluoride ions were determined. It was considered that equilibrium was reached when the fluoride concentration obtained was the same, or that there was a difference of 5% over the earlier recorded period.

The adsorption isotherms were obtained by mixing solutions containing 7.5 g/L of γ-Al_2O_3 or AA, and 0 to 20 mg/L of F^- for 2 h. The suspension also contained 1:1 volume of total ionic strength adjustment buffer (TISAB II) solution to control the suspension of pH at 7.0 ± 0.2 and the ionic strength at 0.04 M., a liter of the TISAB II solution contained, 1% acetic acid ($C_2H_4O_2$), 8% sodium acetate ($C_2H_3NaO_2$), 6% sodium chloride (NaCl), <1% Trans-1,2-Diamino cyclohexane tetra acetic acid (CDTA), and >84% deionized water (H_2O). After mixing, the solutions samples were analyzed to obtain the equilibrium F– concentration.

Resuls and Discussion

Powder X-ray diffraction (XRD)

The crystalline properties of synthesized and agglomerate alumina (γ-Al_2O_3) and AA are shown by the XRD pattern of high angle (10°–80° 2θ) in figure 2. The material of γ-Al_2O_3 exhibits some broad crystalline peaks around 35°–40° and especially at 45° and 67º 2θ. This is due to the reflections (of X-rays) from the 311, 400, and 440 crystal planes, in relation with the cubic γ-Al_2O_3, according to JCPDS Card No. 10-0425 (Renuka, Shijina & Praveen, 2012). This revealed that the γ-Al_2O_3 presented a low degree of crystallization. However, the XRD pattern for the AA demonstrated a significant number of peaks, which suggests that more than one phase is present. On the other hand, other peaks that do not fit within the phase γ-Al_2O_3 can be indexed as pseudoboehmite (γ-AlOOH) phase (JCPDS Card No. 21-1307) (Barzegar & Ebadzadeh, 2011). Therefore, the AA material may be composed of γ-Al_2O_3 and pseudoboehmite such as in a main phase, as shown in figure 2 (gray). Due to this, the AA material showed a greater degree of crystallinity compared with γ-Al_2O_3.

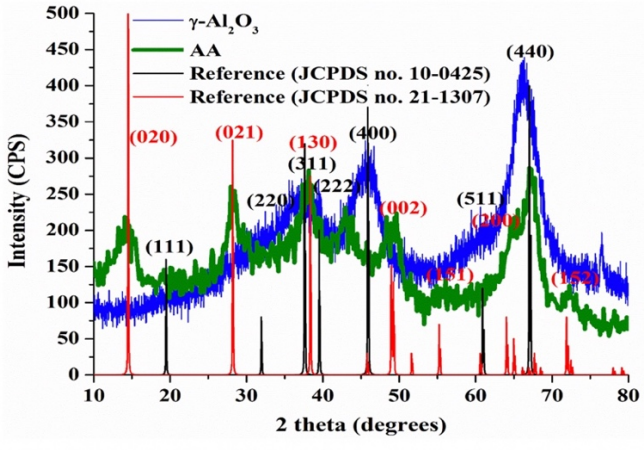

Figure 2. XRD patterns of γ-Al_2O_3 (gray) and AA (black), JCPDS cards: Pseudoboehmite (21-1307), and γ-Al_2O_3 (10-0425).
Source: Author's own elaboration

Adsorption/desorption of N_2

Figure 3 illustrates the N_2 adsorption–desorption isotherms and the Barrett–Joyner–Halenda (BJH) pore size distribution curve of γ-Al_2O_3 and AA. According to the classification made by IUPAC (Sing *et al.*, 1985), the N_2 adsorption–desorption isotherms of γ-Al_2O_3 and AA are found to be of a type IV. Two well distinguished regions in the adsorption isotherm are evident: (i) monolayer–multilayer adsorption and (ii) capillary condensation. The first increase in adsorption at relative pressure P/P0 < 0.2 is due to a multilayer adsorption on the surface, while the second increase at P/P0 = 0.42–0.97 arises from capillary condensation in the mesopores with nitrogen multilayers adsorbed on the inner surface (Gregg, Sing & Salzberg, 1967). These materials show irregular shape isotherms with the hysteresis loop type E, which indicate that the pores in the material have an inkwell-type shape. As seen in figure 3b, a relatively narrow pore size distribution is detected, and the average BJH pore diameter, calculated by using the adsorption branch data of the N_2 adsorption–desorption isotherms, is about 5.8 nm; this measure belongs to the γ-Al_2O_3, and 3.5 nm is the measure for the AA. These values are congruent due to the higher crystallinity that AA presents, as shown in figure 2. Table 1 shows the results of the surface area BET, the pore size distribution, as well as the average pore diameter of γ-Al_2O_3 and AA.

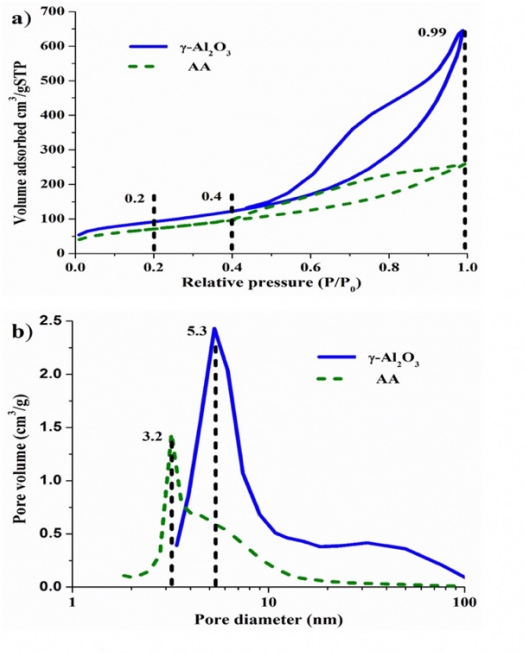

Figure 3. Graphs a) N_2 adsorption–desorption isotherm and b) pore size distribution curve of the γ-Al_2O_3 and AA.
Source: Author's own elaboration.

Table 1. Specific surface area, average pore volume and average pore size of γ-Al_2O_3 and AA.

Sample	SSA (m2•g-1)a	VP (cm3 •g-1)b	DP (nm)c
γ-Al_2O_3	256	0.76	5.8
AA	206	0.39	3.5

[a] Calculated with the BET-equation.
[b] Measured at $p/p_0 = 0.99$.
[c] Pore diameter determined using desorption isotherms by the BJH method.
Source: Author's own elaboration.

Morphology and surface composition of the adsorbents

Figure 4 shows the FE-SEM images of γ-Al_2O_3 and AA. The powder from the γ-Al_2O_3 obtained through the process of hydrolysis-precipitation and agglomerates consists of nanofibers, which are about 100 nm in length. That tends to form amorphous agglomerates due to their high surface energy. Therefore, high porosity is generated. In comparison with the morphology of the commercial AA powder (figure 4b), the powder exhibits a higher degree of agglomeration in the surface and, consequently, it has a lot of small pores.

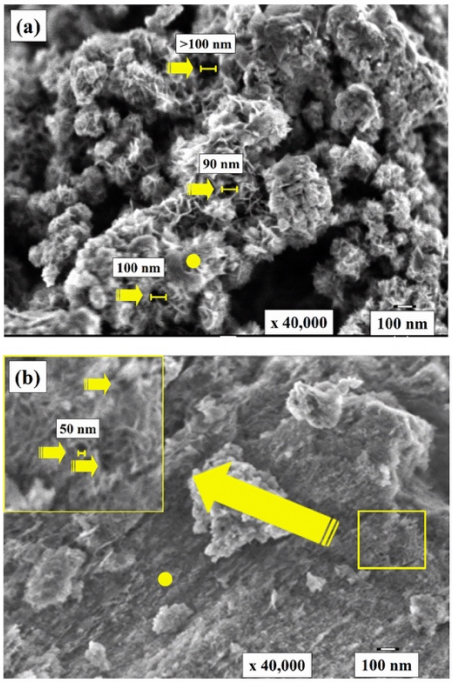

Figure 4. FE-SEM/EDS images of a) γ-Al_2O_3 and b) AA.
Source: Author's own elaboration.

The FE-SEM images of γ-Al_2O_3 and AA (figure. 4) show the spots in places where the electron beam determined the elemental EDS (energy dispersive X-ray spectroscopy) through the analysis. The EDS is employed to identify the elemental compositions from both alumina materials. This technique can be applied to investigate the properties of a broad range of chemicals. Elemental concentrations of aluminum and oxygen are investigated using EDS at one point from both samples. The weight concentrations of both samples are compared in table 2. The analysis confirms the high purity of the alumina samples. The values obtained in the elemental chemical composition of aluminum and oxygen from both samples are congruent with values reported in the literature related to pure alumina (Ilyas, Pendyala, Narahari & Susin, 2017).

Table 2. EDS elemental analysis of γ-Al_2O_3 and AA.

	Element [wt. %]	
Sample	Oxygen	Aluminum
γ-Al_2O_3	54.3	45.7
AA	51.852	44.665

Source: Author's own elaboration.

^{27}Al MAS NMR

Figure 5 displays the ^{27}Al MAS NMR spectra that belong to the γ-Al_2O_3 and AA. The first one is figure 5a, which exhibits characteristic profiles of γ-Al_2O_3, such as signals between 0 ppm and 5 ppm from the octahedral aluminum Al^{VI} sites. Moreover, the presence of signals in the region that are around 34 ppm is evident. This can be associated to aluminum in pentacoordinate sites Al^{V}, and signals between 58 ppm and 62 ppm from the sites of aluminum in tetrahedral geometry Al^{IV}. The second material (figure 5b) exhibits signals between 0 ppm and 5 ppm from the octahedral aluminum Al^{VI} sites, and it signals between 58 ppm and 62 ppm from the aluminum in tetrahedral geometry Al^{IV} sites (Hill, Bastow, Celotto & Hill, 2007; Li, Liu & Liu, 2013). For the sample AA, no resonance related to Al^{V} was found. The integration reveals values between 15% and 20% from the tetrahedral sites, which are in accordance with the γ-Al_2O_3 model (Chagas *et al.*, 2014). The γ-Al_2O_3, as seen in figure 5a, exhibited aluminum pentacoordinate sites Al^{V} which, according to the literature, arise from the structure defects from γ-Al_2O_3. Also, a high Al^{V} amount implies low crystallinity (Tsyganenko & Mardilovich, 1996). The ratio of tetrahedral to octahedral Al is about 1:3, a characteristic from the γ-Al_2O_3 phase (Sifontes *et al.*, 2014).

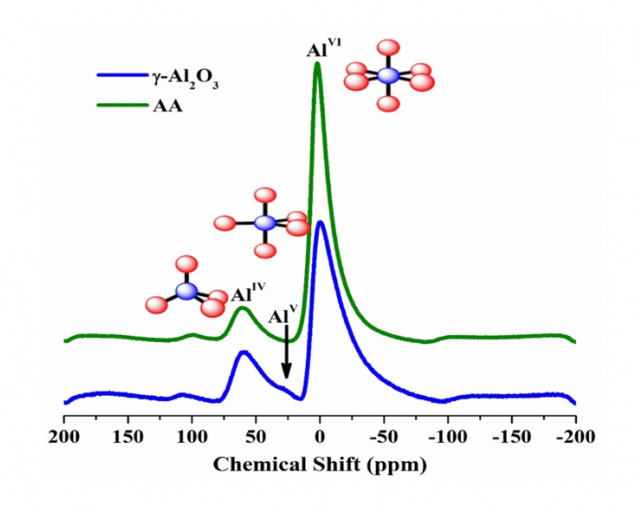

Figure 5. ^{27}Al NMR spectra of γ-Al_2O_3 and AA.
Source: Author's own elaboration.

FT-IR pyridine adsorption

The spectra of the pyridine adsorption–desorption were obtained for the γ-Al_2O_3 and AA at a temperature of 25 ºC, as shown in figure 6. This indicates that only Lewis acid sites were detected, but no Brönsted acid sites were observed from the γ-Al_2O_3. It was possible to observe the IR bands at 1593 cm^{-1}, 1575 cm^{-1}, and 1445 cm^{-1}, which is specific from the vibration mode of pyridine when interacting with medium or weak Lewis acid sites (Liu, 2008; Rana, Huidobro, Ancheyta & Gómez, 2005). Besides the already mentioned bands, other band was observed at 1615 cm^{-1}, associated at pyridine adsorbed on Lewis acid sites. On the other hand, for the adsorbent AA, a band at 1489 cm^{-1} associated with pyridine adsorbed on both Lewis and Brönsted acid sites was observed (Li *et al.*, 2013; Xue, Li, Wang, Liu & Xu, 2010). The results may be relative to the unsaturated alumina atoms (Al^{IV} and Al^{V}) and the specific surface alumina areas. It is agreed that the weak Lewis acidity mainly arises from pentacoordinate aluminum atoms while the medium strong Lewis acidity mainly relates to aluminum atoms in tetrahedral geometry (Li *et al.*, 2013). This is corroborated in figure 5. These features influence directly the surface acidity distribution of γ-Al_2O_3 and AA. As

ISSN online 2007-9621
Romero-Toledo, R., Ruis-Santos, V., Zurita-Luna, U., Rangel-Porras, G., & Martínez-Rosales, M.
Aplication of sheroidal agglomerates of *y*-Al_2O_3 in the fluoride removal from aqueous medium. | 1-16

demonstrated in figure 6, the material AA presents a higher percentage of Brönsted acidity and, according to reported studies, this benefits the fluorine adsorption reaction. That is due to the proton donation.

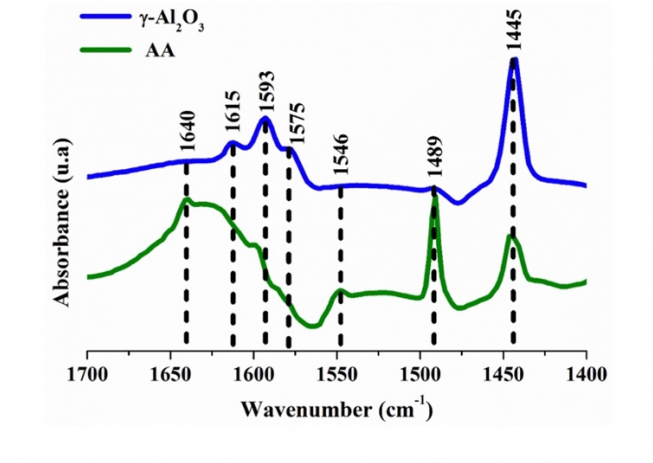

Figure 6. FT-IR spectra of the pyridine adsorption of the γ-Al_2O_3 and AA.
Source: Author's own elaboration.

Zeta potential and particle size

The plot of pH versus zeta potential seen in figure 7 shows the zeta potential measurement of the γ-Al_2O_3 and AA. Specifically, the adsorption capacity of a material is determined by its chemical composition and distribution in a particle surface charge. Zeta potential (PZ) is widely used for electrical charge magnitude quantification in a double layer (Wang & Keller, 2009). The isoelectric point of AA and γ-Al_2O_3 is found at pH 8.6 and 7.72, respectively. This is consistent with the reported data in the literature. This indicates that the synthesized and agglomerate alumina surface is slightly basic. This result corroborates that the basic sites concentration is slightly higher for the γ-Al_2O_3 than AA, as determined by FT-IR pyridine adsorption (figure 6). The reported values show that the potential zeta for AA or γ-Al_2O_3 are around pHPZC 8.94 (Cheng *et al.*, 2014). In other researches, different pHPZC values were reported: 8.3 (Bowen, Carry, Luxembourg & Hofmann, 2005), 8.5 (Zamorategui, Ramírez, Martínez & Serafín, 2016), 8.0 for a commercial AA (Ku & Chiou, 2002), and (Choi & Chen, 1979) reported that the pHPZC, which belongs to the adsorbents AA, ranged from 6.2 to 8.9. Therefore, the PZ pertaining to synthesized and agglomerate alumina and commercial AA, which was employed in this work, was within the range of values reported in the literature. These potential changes are related to the flocculation phenomena and the neutralized surface charge. The differences in the values of IEP are attributed to the acidity from both materials. This acidity depends on the coordination of aluminum atoms, as observed in figure 5; this is due to change in surface charge. The AA presented a higher acidity due to the presence of Lewis and Brönsted acid sites, in comparison with the γ-Al_2O_3. This can be observed in the FT-IR spectra of the pyridine adsorption. Figure 7b shows the size of particles that belongs to the γ-Al_2O_3 (0.27 μm) and AA (0.5 μm). The particle size of γ-Al_2O_3 is smaller than that of the AA. This is due to a combination of phases, such as gamma-alumina and pseudoboehmite as the main phase. Their entirety was not affected by dehydration and agglomeration of crystals.

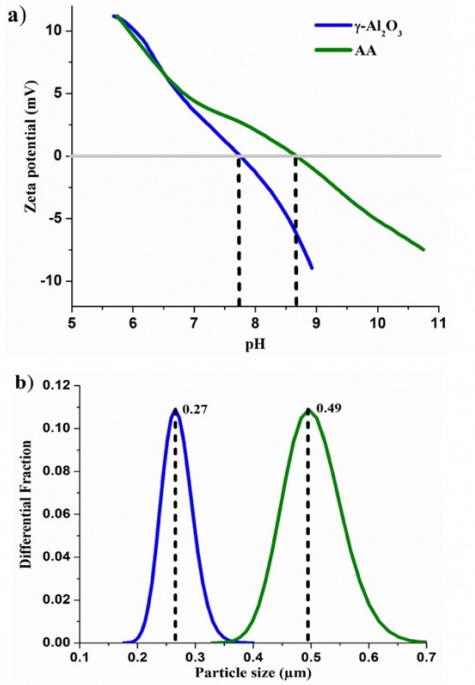

Figure 7. Graphs of a) potential zeta, b) particle size of the γ-Al_2O_3, and AA.
Source: Author's own elaboration.

Adsorption isotherms of fluoride

Adsorption depends on ions in fluid (adsorbate), which diffuses through the solid surface (adsorbent). In this surface, they bond or are held there by weak intermolecular forces (Li *et al*., 2011). Adsorption studies pointed out the most important characteristics which determined adsorbent suitability for practical applications: the adsorption capacity, selectivity for fluoride ions, regenerability, compatibility, particle and pore size, and low cost. It is important to consider that fluoride removal efficiency always depends on a raw water quality profile, i.e., initial fluoride concentration, pH, temperature, contact time, and adsorbent dosage (Bhatnagar *et al.*, 2011; Mohapatra, Anand, Mishra, Giles & Singh, 2009; Rao, 2003; Tomar & Kumar, 2013). The Langmuir adsorption model is the most common model used to quantify the amount of adsorbate on an adsorbent as a function of partial pressure or concentration at a given temperature. Adsorption isotherms for the γ-Al_2O_3 and AA are shown in figure 8, and these go in accordance with the Langmuir equation which is represented as:

$$C_e / q_e = 1/ q_m + 1/ q_m b C_e \quad (3)$$

In this equation, q_e (mg • g-1) is the solution that was adsorbed by the surface, b is the constant equilibrium of adsorption, and q_m is the capacity of adsorption in a saturated single layer. Finally, C_e (mg • l-1) is the solution in equilibrium state (Rahimi & Vadi, 2014).

Figure 8 illustrated the adsorption isotherms of γ- Al_2O_3 and AA. Figure 8a shows the adsorption isotherms of F– in the γ-Al_2O_3 and AA at 25 ºC, at pH 5, 7, and 9. The results indicate a higher capacity of adsorption from γ-Al_2O_3 than AA at pH 5, approximately 15 mg of F-/g and 11 mg of F-/g, respectively. Figure 8b shows the adsorption isotherms of F– from the γ-Al_2O_3 and AA at 35 ºC, at pH 5, 7, and 9. These

results indicate a slightly higher capacity of adsorption for γ-Al_2O_3 than for AA at pH 5. That is approximately 12 mg in F-/g and 11 mg in F-/g, respectively. The best-fit parameters are listed in table 3 and 4. The adsorption capacity results for γ-Al_2O_3 at pH 7 are approximately 10 mg of F-/g and 9 mg of F-/g for AA at 25 ºC. Moreover, at 35 ºC, the adsorption capacity of 8 mg in F-/g and 9 mg in F-/g was revealed. The qmax value for AA was 16.7 mg/g. The γ-Al_2O_3 with a q_{max} (27.5 mg/g) had a much higher level than the AA at 25 ºC. The qmax value for AA was 15.3 mg/g. The γ-Al_2O_3 presented a q_{max} (23.3 mg/g), which had a much higher level than the AA, at 35 ºC and at pH 5. In this study, solutions of 50 ppm of fluoride ion were used.

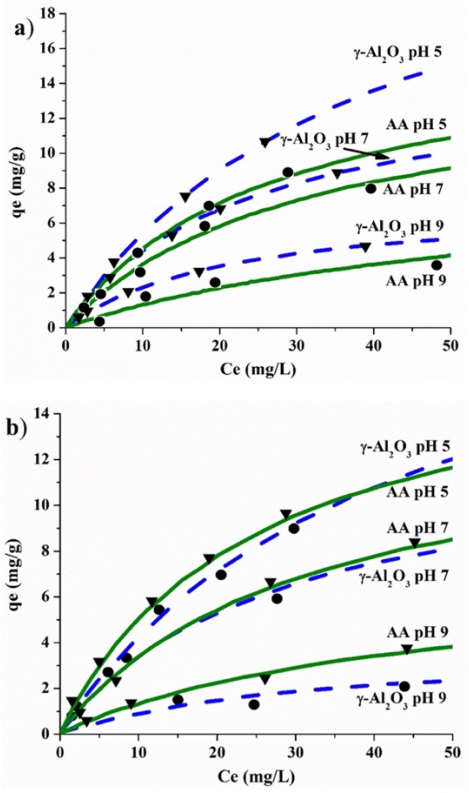

Figure 8. Adsorption isotherms of fluoride of γ-Al_2O_3 and AA, at a) 25 ºC and b) 35 ºC, at pH different.
Source: Author's own elaboration.

Table 3. Parameters and correlation coefficient of Langmuir equation (pH 5, 7, and 9, at 25 ºC).

Sample	K (L/mg)	Q_{max} (mg/g)	R (corr.)	Langmuir equation
(pH 5)				
γ-Al_2O_3	0.0244	27.5200	98.99	qe=(0.0244)•(27.5200Ce)/(1+0.0244Ce)
AA	0.0371	16.7319	99.57	qe=(0.0371)•(16.7319Ce)/(1+0.0371Ce)
(pH 7)				
γ-Al_2O_3	0.0421	14.9654	99.52	qe=(0.0421)•(14.9654Ce)/(1+0.0421Ce)
AA	0.0319	14.8116	99.88	qe=(0.0319)•(14.8116Ce)/(1+0.0319Ce)
(pH 9)				
γ-Al_2O_3	0.0458	7.3031	98.87	qe=(0.0458)•(7.3031Ce)/(1+0.0458Ce)
AA	0.0163	9.1748	99.50	qe=(0.0163)•(9.1748Ce)/(1+0.0163Ce)

Source: Author's own elaboration.

ISSN online 2007-9621

Table 4. Parameters and correlation coefficient of Langmuir equation (pH 5, 7, and 9, at 35 ºC).

Sample	K (L/mg)	Q_{max} (mg/g)	R (corr.)	Langmuir equation
(pH 5)				
γ-Al_2O_3	0.0210	22.3138	99.12	qe=(0.0210)•(22.3138Ce)/(1+0.0210Ce)
AA	0.0364	15.3703	99.21	qe=(0.0364)•(15.3703Ce)/(1+0.0364Ce)
(pH 7)				
γ-Al_2O_3	0.0332	12.5148	98.65	qe=(0.0332)•(12.5148Ce)/(1+0.0332Ce)
AA	0.0293	13.7077	98.76	qe=(0.0293)•(13.7077Ce)/(1+0.0293Ce)
(pH 9)				
γ-Al_2O_3	0.0261	3.9344	98.17	qe=(0.0261)•(3.9344Ce)/(1+0.0261Ce)
AA	0.0199	7.1792	99.14	qe=(0.0199)•(7.1792Ce)/(1+0.0199Ce)

Source: Author's own elaboration.

The results indicated that the commercial agglomerate AA presented a higher crystallinity than the γ-Al_2O_3, synthesized and agglomerate. This is attributed to what is shown in a diffractogram from a hybrid material that belongs to a γ-Al_2O_3 and a pseudoboehmite as a main phase (> %). On the other hand, the adsorption of fluoride ions occurs on the surface of the adsorbent material. Adsorption process is controlled by the diffusion of the fluoride ion in the liquid, and the fluoride ion must diffuse into the adsorbent agglomerate. This is the reason why the amount of fluoride ion adsorbed is less for the AA than for the γ-Al_2O_3, since the phenomenon is influenced by the size of the pores through which the fluoride ion is transported. The fluoride was adsorbed in the active sites of the activated alumina that are formed in the aluminum atoms of the alumina framework. No adsorption studies at a lower pH were explored due to the loss of active sites. The reason for this is the dissolution of aluminum present in the alumina.

The capacity of the alumina materials for adsorbing the fluoride was considerably dependent of the solution pH. The effect of the solution pH in the adsorption capacity can be ascribed to the electrostatic or coulombic interactions between the alumina surface and the fluoride ions in the aqueous solution. The γ-Al_2O_3 and AA surface was charged positively at a pH level lower than the PZC of 7.72 and 8.6, respectively. Hence, the fluoride ion was attracted to both materials' surface. On the contrary, the surface was negatively charged at a pH level higher than 7.72 and 8.6. Hence, the fluoride ion was repelled from the surface.

Conclusion

The γ-Al_2O_3 synthesized by the hydrolysis-precipitation method and agglomerate has effective properties to be considered as an adsorbent material, which can be used to remove the fluoride ion present in drinking water from columns of adsorption at industrial sites. The γ-Al_2O_3 particles had a small zeta potential and a great adsorption capacity compared with the AA particles at the same pH and temperature. The adsorption behavior of γ-Al_2O_3 and AA was well described with the pseudo-first-order kinetics, and the adsorption isotherms were described with the Langmuir equation. The maximum adsorption capacities of γ-Al_2O_3 and AA determined by the Langmuir equation were 15 mg/g and 11 mg/g at pH = 5.0, at 25 ºC, respectively. The optimum pH for F– removal by the adsorbents was 5. The γ-Al_2O_3 synthesized and agglomerate demonstrated to be a more effective adsorbent than the commercial and commonly used AA for F– removal from water.

Acknowledgements

Authors gratefully acknowledge the support provided by the National Council on Science and Technology (Conacyt, from its Spanish Initials), LICAMM UG: Laboratory of research and characterization of minerals and material, for providing access to XRF and XRD and the University of Guanajuato, Mexico; and to Dra. Aida Gutierrez Alejandre, for the support for the realization of the analysis of FT-IR pyridine adsorption, UNICAT, Universidad Nacional Autónoma de México (UNAM).

References

Arahman, N., Mulyati, S., Lubis, M. R., Takagi, R., & Matsuyama, H. (2016). The removal of fluoride from water based on applied current and membrane types in electrodialyis. *Journal of Fluorine Chemistry*, *191*, 97-102. doi: https://doi.org/10.1016/j.jfluchem.2016.10.002

Arora, M., & Maheshwari, R. C. (2006). Fluoride in drinking water and its removal. *Journal of Hazardous Materials*, *137*(1), 456-463. doi: https://doi.org/10.1016/j.jhazmat.2006.02.024

Barzegar-Bafrooei, H., & Ebadzadeh, T. (2011). Synthesis of nanocomposite powders of γ-alumina-carbon nanotube by sol–gel method. *Advanced Powder Technology*, *22*(3), 366-369. doi: https://doi.org/10.1016/j.apt.2010.05.005

Bhatnagar, A., Kumar, E., & Sillanpää, M. (2011). Fluoride removal from water by adsorption a review. *Chemical Engineering Journal*, *171*(3), 811-840. doi: https://doi.org/10.1016/j.cej.2011.05.028

Bowen Paul, Carry Claude, Luxembourg David, Hofmann Heinrich. (2005). Colloidal processing and sintering of nanosized transition aluminas. *Powder Technology*, *157*(1–3), 100-107. doi: https://doi.org/10.1016/j.powtec.2005.05.015

Chagas, L. H., De Carvalho, G. S. G., San Gil, R. A. S., Chiaro, S. S. X., Leitão, A. A., & Diniz, R. (2014). Obtaining aluminas from the thermal decomposition of their different precursors: An ^{27}Al MAS NMR and X-ray powder diffraction studies. *Materials Research Bulletin*, *49*, 216-222. doi: https://doi.org/10.1016/j.materresbull.2013.08.072

Chatterjee, S., & De, S. (2014). Adsorptive removal of fluoride by activated alumina doped cellulose acetate phthalate (CAP) mixed matrix membrane. *Separation and Purification Technology*, 125, 223–238. doi: https://doi.org/10.1016/j.seppur.2014.01.055

Cheng, J., Meng, X., Jing, C., & Hao, J. (2014). La^{3+} modified activated alumina for fluoride removal from water. *Journal of hazardous materials*, *278*, 343-349. doi: https://doi.org/10.1016/j.jhazmat.2014.06.008

Choi, W. W., & Chen, K. Y. (1979). The removal of fluoride from waters by adsorption. *Journal American Water Works Association, 71*(10), 562-570. doi: https://doi.org/10.1002/j.1551-8833.1979.tb04420.x

Diario Oficial de la Federación (DOF). (2001). Norma Oficial Mexicana NOM-127-SSA1-1994. *Salud ambiental. Agua para uso y consumo humano. Límites permisibles de calidad y tratamientos a que debe someterse el agua para su potabilización*. Secretaría de Salud (SS).

Drouiche, N., Aoudj, S., Lounici, H., Drouiche, M., Ouslimane, T., & Ghaffour, N. (2012). Fluoride removal from pretreated photovoltaic wastewater by electrocoagulation: an investigation of the effect of operational parameters. *Procedia Engineering*, *33*, 385-391. doi: https://doi.org/10.1016/j.proeng.2012.01.1218

Ghorai, S., & Pant, K. K. (2005). Equilibrium, kinetics and breakthrough studies for adsorption of fluoride on activated alumina. *Separation and purification technology*, *42*(3), 265-271. doi: https://doi.org/10.1016/j.seppur.2004.09.001

Gómez-Hortigüela, L., Pérez-Pariente, J., García, R., Chebude, Y., & Díaz, I. (2013). Natural zeolites from Ethiopia for elimination of fluoride from drinking water. *Separation and Purification Technology*, *120*, 224-229. doi: https://doi.org/10.1016/j.seppur.2013.10.006

Gregg, S. J., Sing, K. S. W., & Salzberg, H. W. (1967). Adsorption surface area and porosity. *Journal of the Electrochemical Society*, *114*(11), 279C. doi: 10.1149/1.2426447

Guo, Q., & Tian, J. (2013). Removal of fluoride and arsenate from aqueous solution by hydrocalumite via precipitation and anion exchange. *Chemical engineering journal*, *231*, 121-131. doi: https://doi.org/10.1016/j.cej.2013.07.025

Hill, M. R., Bastow, T. J., Celotto, S., & Hill, A. J. (2007). Integrated study of the calcination cycle from gibbsite to corundum. *Chemistry of materials*, *19*(11), 2877-2883. doi: https://doi.org/10.1021/cm070078f

Ilyas, S. U., Pendyala, R., Narahari, M., & Susin, L. (2017). Stability, rheology and thermal analysis of functionalized alumina-thermal oil-based nanofluids for advanced cooling systems. *Energy Conversion and Management*, *142*, 215-229. doi: https://doi.org/10.1016/j.enconman.2017.01.079

Jadhav, S. V., Marathe, K. V., & Rathod, V. K. (2016). A pilot scale concurrent removal of fluoride, arsenic, sulfate and nitrate by using nanofiltration: Competing ion interaction and modelling approach. *Journal of Water Process Engineering*, *13*, 153-167. doi: https://doi.org/10.1016/j.jwpe.2016.04.008

Kir, E., & Alkan, E. (2006). Fluoride removal by Donnan dialysis with plasma-modified and unmodified anion-exchange membranes. *Desalination*, *197*(1-3), 217-224. doi: https://doi.org/10.1016/j.desal.2006.01.018

Ku, Y., & Chiou, H. M. (2002). The adsorption of fluoride ion from aqueous solution by activated alumina. *Water, air, and soil pollution*, *133*(1-4), 349-361. doi: https://doi.org/10.1023/A:1012929900113

Leyva-Ramos, R., Medellin-Castillo, N. A., Jacobo-Azuara, A., Mendoza-Barron, J., Landin-Rodriguez, L. E., Martinez-Rosales, J. M., & Aragon-Piña, A. (2008). Fluoride removal from water solution by adsorption on activated alumina prepared from pseudo-boehmite. *Journal Environmental Engineering Management*, *18*(5), 301-309.

Li, G., Liu, Y., & Liu, C. (2013). Solvothermal synthesis of gamma aluminas and their structural evolution. *Microporous and Mesoporous Materials*, *167*, 137-145. doi: https://doi.org/10.1016/j.micromeso.2012.09.005

Li, Y. H., Wang, S., Cao, A., Zhao, D., Zhang, X., Xu, C., Luan, Z., Ruan, D., Liang, J., Wu, D., & Wei, B. (2001). Adsorption of fluoride from water by amorphous alumina supported on carbon nanotubes. *Chemical Physics Letters*, *350*(5), 412-416. doi: https://doi.org/10.1016/S0009-2614(01)01351-3

Li, Y., Zhang, P., Du, Q., Peng, X., Liu, T., Wang, Z., Xia, Y., Zhang, W., Wang, K., Zhu, H., & Wu, D. (2011). Adsorption of fluoride from aqueous solution by graphene. *Journal of Colloid and Interface Science*, *363*(1), 348-354. doi: https://doi.org/10.1016/j.jcis.2011.07.032

Liu, X. (2008). DRIFTS study of surface of γ-alumina and its dehydroxylation. *The Journal of Physical Chemistry C*, *112*(13), 5066-5073. doi: https://doi.org/10.1021/jp711901s

Ma, Y., Shi, F., Zheng, X., Ma, J., & Gao, C. (2011). Removal of fluoride from aqueous solution using granular acid-treated bentonite (GHB): Batch and column studies. *Journal of Hazardous Materials*, *185*(2), 1073-1080. doi: https://doi.org/10.1016/j.jhazmat.2010.10.016

Mohapatra, M., Anand, S., Mishra, B. K., Giles, D. E., & Singh, P. (2009). Review of fluoride removal from drinking water. *Journal of Environmental Management*, *91*(1), 67-77. doi: https://doi.org/10.1016/j.jenvman.2009.08.015

Morales, I., Villanueva-Estrada, R. E., Rodríguez, R., Armienta, M. A. (2015). Geological, hydrogeological, and geothermal factors associated to the origin of arsenic, fluoride, and groundwater temperature in a volcanic environment "El Bajio Guanajuatense", Mexico. *Environmental Earth Sciences, 74*(6),5403–5415. doi: https://doi.org/10.1007/s12665-015-4554-9

Nigri, E. M., Bhatnagar, A., & Ferreira-Rocha, S. D. (2017). Thermal regeneration process of bone char used in the fluoride removal from aqueous solution. *Journal of Cleaner Production*, *142*(4), 3558-3570. doi: https://doi.org/10.1016/j.jclepro.2016.10.112

Rafique, A., Awan, M. A., Wasti, A., Qazi, I. A., & Arshad, M. (2012). Removal of fluoride from drinking water using modified immobilized activated alumina. *Journal of Chemistry*, *2013*, 1-7. doi: http://dx.doi.org/10.1155/2013/386476

Rahimi, M., & Vadi, M. (2014). Langmuir, Freundlich and Temkin Adsorption Isotherms of Propranolol on Multi-Wall Carbon Nanotubes. *Journal of Modern Drug Discovery and Drug Delivery Research*, 2, 18-20.

Rana, M. S., Huidobro, M. L., Ancheyta, J., & Gómez, M. T. (2005). Effect of support composition on hydrogenolysis of thiophene and Maya crude. *Catalysis Today*, *107*, 346-354. doi: https://doi.org/10.1016/j.cattod.2005.07.029

Rao, C.R. (2003). Fluoride and environment-A review. In M. J. Bunch, V. M. Suresh, & T. V. Kumaran. *Proceedings of the Third International Conference on Environment and Health* (pp. 386-399), Chennai, India.

Renuka, N. K., Shijina, A. V., & Praveen, A. K. (2012). Mesoporous γ-alumina nanoparticles: synthesis, characterization and dye removal efficiency. *Materials Letters*, *82*, 42-44. doi: https://doi.org/10.1016/j.matlet.2012.05.043

Rogoziński, R., Tyszkiewicz, C., Karasiński, P., Żelechower, M., & Szala, J. (2016). Silica layers as masks in Ag+-Na+ ion exchange processes. *Thin Solid Films*, *615*, 122-127. doi: https://doi.org/10.1016/j.tsf.2016.06.043

Rosales, M., Coreño, O., & Nava, J. L. (2018). Removal of hydrated silica, fluoride and arsenic from ground water by electrocoagulation using a continuous reactor with a twelve-cell stack. *Chemosphere, 211*, 149-155. doi: https://doi.org/10.1016/j.chemosphere.2018.07.113

Sehn, P. (2008). Fluoride removal with extra low energy reverse osmosis membranes: three years of large scale field experience in Finland. *Desalination*, *223*(1-3), 73-84. doi: https://doi.org/10.1016/j.desal.2007.02.077

Shen, C., Wu, L., Chen, Y., Li, S., Rashid, S., Gao, Y., & Liu, J. (2016). Efficient removal of fluoride from drinking water using well-dispersed monetite bundles inlaid in chitosan beads. *Chemical Engineering Journal*, *303*, 391-400. doi: https://doi.org/10.1016/j.cej.2016.05.103

Shen, J., Richards, B. S., & Schäfer, A. I. (2016). Renewable energy powered membrane technology: Case study of St. Dorcas borehole in Tanzania demonstrating fluoride removal via nanofiltration/reverse osmosis. *Separation and Purification Technology*, *170*, 445-452. doi: https://doi.org/10.1016/j.seppur.2016.06.042

Sifontes, Á. B., Gutierrez, B., Mónaco, A., Yanez, A., Díaz, Y., Méndez, F. J., Llovera, L., Cañizales, E., & Brito, J. L. (2014). Preparation of functionalized porous nano γ-Al_2O_3 powders employing colophony extract. *Biotechnology Reports*, *4*, 21-29. doi: https://doi.org/10.1016/j.btre.2014.07.001

Sing, K. S. W., Everett, D. H., Haul, R. A. W., Moscou, L., Pierotti, R. A., Rouquérol, J., Siemieniewska, T. (1985). Reporting physisorption data for gas/solid systems with special reference to the determination of surface area and porosity (Recommendations 1984). *Pure and Applied Chemistry, 57*(4), 603–619. doi: https://doi.org/10.1351/pac198557040603

Singh, J., Singh, P., & Singh, A. (2016). Fluoride ions vs removal technologies: a study. *Arabian Journal of Chemistry*, *9*(6), 815-824. doi: https://doi.org/10.1016/j.arabjc.2014.06.005

Tang, Y., Guan, X., Su, T., Gao, N., & Wang, J. (2009). Fluoride adsorption onto activated alumina: Modeling the effects of pH and some competing ions. *Colloids and Surfaces A: Physicochemical and Engineering Aspects*, *337*(1), 33-38. doi: https://doi.org/10.1016/j.colsurfa.2008.11.027

Tomar, V., & Kumar, D. (2013). A critical study on efficiency of different materials for fluoride removal from aqueous media. *Chemistry Central Journal*, *7*(1), 1. doi: https://doi.org/10.1186/1752-153X-7-51

Tor, A. (2006). Removal of fluoride from an aqueous solution by using montmorillonite. *Desalination*, *201*(1-3), 267-276. doi: https://doi.org/10.1016/j.desal.2006.06.003

Tsyganenko, A. A., & Mardilovich, P. P. (1996). Structure of alumina surfaces. *Journal of the Chemical Society, Faraday Transactions*, *92*(23), 4843-4852. doi: https://doi.org/10.1039/FT9969204843

Wang Qilin, Jiang Guangming, Ye Liu, Yuan Zhiguo. (2014). Enhancing methane production from waste activated sludge using combined freenitrous acid and heat pre-treatment. Water Research, *63*, 71-80. doi: https://doi.org/10.1016/j.watres.2014.06.010

Wang, P., & Keller, A. A. (2009). Natural and engineered nano and colloidal transport: role of zeta potential in prediction of particle deposition. *Langmuir*, *25*(12), 6856-6862. doi: https://doi.org/10.1021/la900134f

World Health Organization (WHO). (2004). Guidelines for drinking-water quality (3rd Ed.). Switzerland: WHO, Geneva.

Xu, B., Yang, Y., Xu, Y., Han, B., Wang, Y., Liu, X., & Yan, Z. (2017). Synthesis and characterization of mesoporous Si-modified alumina with high thermal stability. *Microporous and Mesoporous Materials*, *238*, 84-89. doi: https://doi.org/10.1016/j.micromeso.2016.02.031

Xue, B., Li, Y., Wang, S., Liu, H., & Xu, C. (2010). Selective synthesis of ethylbenzene by alkylation of benzene with diethyl carbonate over MCM-22 modified by MgO. *Reaction Kinetics, Mechanisms and Catalysis*, *100*(2), 417-425. doi: https://doi.org/10.1007/s11144-010-0198-7

Yeung, C. A. (2008). A systematic review of the efficacy and safety of fluoridation. *Evidence-Based Dentistry*, *9*(2), 39-43. doi: https://doi.org/10.1038/sj.ebd.6400578

Zamorategui, A., Ramírez, N., Martínez, J. M., & Serafín, A. H. (2016). Synthesis and characterization of gamma alumina and compared with an activated charcoal on the fluoride removal from potable well water. *Acta Universitaria*, *26*(2), 30-35. doi: 10.15174/au.2016.878